Hindawi
Advances in Civil Engineering
Volume 2019, Article ID 4942578, 11 pages
https://doi.org/10.1155/2019/4942578

Research Article

Evaluation of Geomembrane Effect Based on Mobilized Shear Stress due to Localized Sinking

Weihua Lu,[1,2,3] **Yongxing Zhang**,[4] **Weizheng Liu**,[5] **Cheng Liu**,[1] **and Haibo Wang**[1]

[1]*Associate Professor, School of Civil Engineering, Nanjing Forestry University, No. 159 Longpan Road, Nanjing, Jiangsu 210037, China*
[2]*Key Laboratory of Road Structure and Material of Ministry of Transport (Changsha), Changsha University of Science & Technology, Changsha 410114, Hunan, China*
[3]*Guangxi Key Laboratory of Disaster Prevention and Engineering Safety, Key Laboratory of Disaster Prevention and Structural Safety of Ministry of Education, Guangxi University, Nanning, China*
[4]*Professor, Guangxi Key Laboratory of Disaster Prevention and Engineering Safety, Key Laboratory of Disaster Prevention and Structural Safety of Ministry of Education, Guangxi University, Nanning, China*
[5]*Associate Professor, School of Civil Engineering, Central South University, No. 22 Shaoshan South Road, Tianxin District, Changsha, Hunan 410075, China*

Correspondence should be addressed to Weizheng Liu; liuwz2011@csu.edu.cn

Received 24 November 2018; Revised 28 February 2019; Accepted 18 April 2019; Published 2 May 2019

Academic Editor: Annan Zhou

Installing geosynthetic reinforcement at the bottom of the embankment will provide positive support for subgrade stability and settlement control, if there is a void or a weak foundation. In routine design work, the geomembrane effect must be well estimated and the tensile strain should be precisely predicted. Conventional analytical methods often adopt the limit state method to calculate the overlying load on the deflected geosynthetic. However, this assumption does not necessarily apply to all conditions, especially when the foundation soil can provide certain resistance. In this study, a semiempirical prediction method for evaluating the geomembrane effect of the basal reinforcement was proposed, and an iterative solution for calculating tensile strains of a deflected geosynthetic was deduced. In derivation, a virtual inclined slip surface and interaction between the geosynthetic and soil were quantitatively evaluated by coupling the arching effect and the geomembrane effect. Moreover, the development of shear stress along the slip surface can be considered, as well as different segments of the basal reinforcement. Then, the proposed method was validated by two large-scale experiments. Comparison of the results of this method with measurements and results of other analytical models confirmed that this analytical method can take good care of the varying process of the localized sinking, regarding the overlying loads on the geosynthetic and the subsequent tensile strains.

1. Introduction

Constructing road embankments on soft soil foundation, or there exists sinkholes or voids underneath, faces the threat of excessive settlement or different settlement. Although lightweight fill, piles, and subgrade enhancing technologies are always adopted to solve the problem, as well as other engineering issues, implementing a geosynthetic is often necessary to reduce settlement and enhance stability [1–7]. In reinforced structures, the geosynthetic mainly plays a load redistribution role between the subsided zone and the surrounding less-deformed zone. Moreover, the geomembrane effect always occurs along with the soil arching effect. Subjected to local subsidence at the fill base, the overlying fill deflects the basal reinforcement and is also prevented from subsiding by the geosynthetic simultaneously. Aiming to desire a reasonable design of the reinforced structure, an important task is to accurately evaluate the geomembrane effect, i.e., calculate the tensile strains. However, it is not practical to consider the tension of a geosynthetic solely without investigating the overlying loads. Therefore, the arching effect and the geomembrane effect,

both of which are key design points, should be quantitatively evaluated. The former is to obtain the load acted on the geosynthetic, while the latter is to determine the maximum tensile strain of the installed geosynthetic.

In general, the portrayals used for depicting soil arches can be divided into two categories. One is to derive the static stress balance of a horizontal thin strip analysis unit in the vertical direction, represented by the Terzaghi [8] method. The other is to deduce the stress expression of the loosening zone of Earth pressure influenced by arching based on different nonvertical curvilinear slip surfaces [9, 10]. Arching behavior is always influenced by the geomembrane effect and the resistance from the compressible subsoil [11–14]. For the family of frictional arching models, the shear stress along the slip surface is mainly dependent on the differential settlement at the fill base. Several methods have been found in the literature for evaluating the mechanism of shear friction that is significantly affected by arch behaviors or geosynthetic layers [15–18]. Those methods are usually calculated in two steps: the first is to deduce the pressure, and the second is to compute the tensile strain of the geosynthetic subjected to the previous computational pressure.

Based on the fixed geometry assumption (such as circular, parabolic, or their combination), traditional geomembrane evaluation methods usually consider that the geosynthetic layer is fixed at one edge and the tensile strain is uniformly distributed within the full-length range [16, 19, 20]. Moreover, the tensile strain is only dependent on the ratio of the reinforcement's deflection to the cavity diameter or subsiding width, instead of the overburden load and other material properties. However, nonuniform distribution and peak strain existence within the geosynthetic reinforcement have been gradually confirmed in real scenarios and numerical simulations [21–24], indicating that the working condition of the horizontal installed reinforcement should be characterized more realistically. Then, improved evaluation methods are strongly recommended, and more factors (such as the interfacial friction between the fill material and reinforcement) have to be considered in the geomembrane effect [25–29].

In a low embankment, as the two-dimensional stress state is considered, the settlement area at the top of the embankment is larger than that of the base. This indicates that the slip surface of the subsiding embankment fill against the motionless part resting on both sides undergoes a process of changing from the vertical direction to inclined directions. Therefore, the reinforcing behavior of the geosynthetic layer is quite different from the conventional ideas, accounting for the soil arching effect by utilizing a vertical [8], a spiral [30], a semicircular [31, 32], or a triangular [33] physical model presented by the aforementioned literature. Using a similar configuration, the aim of this study is to present a calculation method for the geomembrane effect with regard to nonuniform tensile strain of the geosynthetic reinforcement. In derivation, an improved arching mechanism based on mobilized shear stress within the inclined slip surface is evaluated, as well as the identified reinforcing mechanism of the horizontal geosynthetic layer. Finally, the method is validated by two physical model tests.

2. Developing Arching Effect on Nonvertical Slip Surface

Figure 1 illustrates a profile of a 2D analytical model of the basal reinforced embankment subjected to localized sinking. The subsidence width at the base and top are b and B_s, respectively. The height of the fill is H. Terzaghi [8] has pointed out that the angle of the inclined slip surface would vary from 90° to $45 + \varphi/2$ with the increasing ratio of H to b of the fill mass in the famous trapdoor test. Therefore, a vertical slip surface assumption would not be fully conformed to the actual situation in a low fill mass, and the subsidence basin would extend to a degree due to material cohesion or internal friction angle of the fill. Then, boundary trajectories of the slip surfaces can be simplified by two curves, a′b and cd′, with an inclined angle α to the vertical direction.

In Figure 2, a soil strip element ABC at the bottom, representing the mechanical behavior of the fill within the stress release region due to arching, is selected to conduct the equilibrium analysis of vertical stresses. The soil strip element can be idealized as a simple beam that is supported at two pivot points. The deflection of the soil element is assumed to be δ, and the deflection angle at point A is θ. The positive stress perpendicular to the slip surface is σ_{ns}, and the shear stress is τ_s. Different from the definition of lateral Earth pressure coefficient K proposed by Krynine [34], the coefficient here changes with the position along the slip surface and is also related to the internal friction angle φ of the fill material.

Figure 3 shows a mobilized stress Mohr circle, in which the shear stress along the slip surface varies, to represent the stress state of a position starting from the edge of the basal subsiding area to the fill top surface. In traditional arching theory, the soil stress state along the slip surface is always considered to have reached the limit state. Therefore, the results calculated by the above limit state methods are always conservative, and their assumptions and factors are prone to fly in the face of the real scenario. It is believed that the magnitude of the shear stress along the slip surface is mainly dependent on the relative displacement at the fill base. Typically, when the embankment fill height is not high enough, or if the foundation soil underneath the geosynthetic provides a certain resistance, the Mohr circle will not be tangent to the shear strength envelope. In other words, an incomplete soil arching effect occurs, indicating that the maximum shear stress is lower than the ultimate shear strength.

Based on the above analytical assumptions, a unit length perpendicular to the paper direction is selected for a simplification of the two-dimensional stress equilibrium condition. At a depth z to the top surface within the subsided area, the width of the soil strip unit of EFG is termed as B_z. In the subsequent derivation, the cohesion of the fill material is not considered, and then through the stress equilibrium condition on vertical direction, the following equation can be obtained:

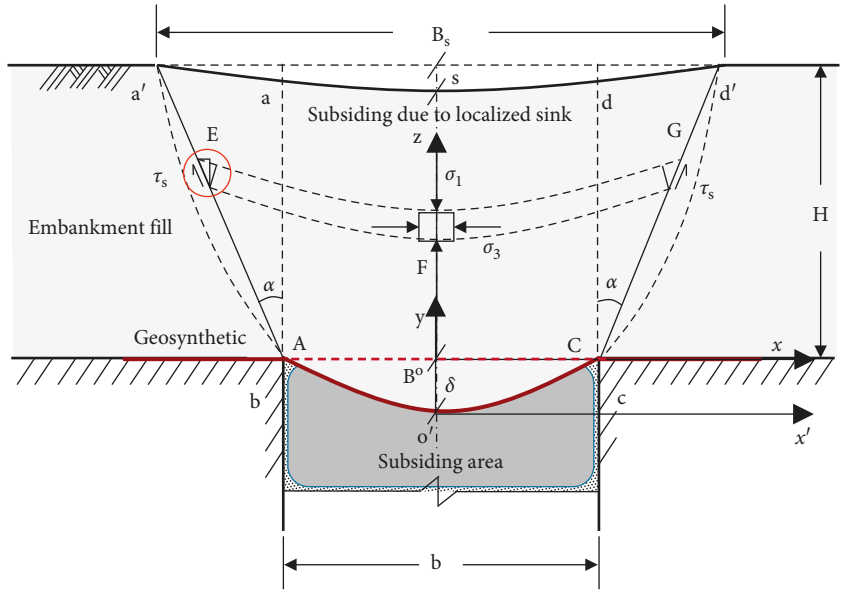

Figure 1: Sketch of a two-dimensional embankment section after local subsiding.

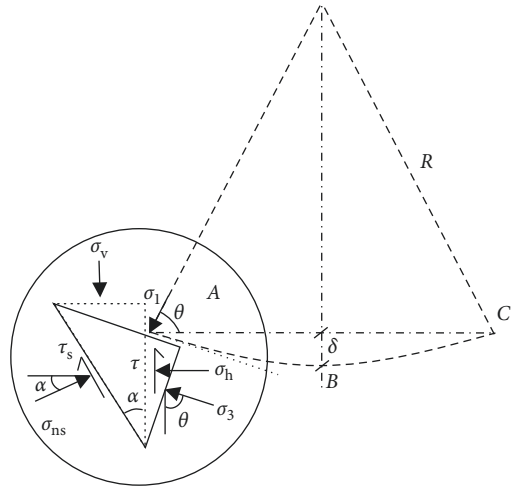

Figure 2: Schematic diagram of stress state analysis of the deflected soil strip element.

$$\sum Y = 0,$$

$$\sigma_v B_z + \gamma dz B_z = (\sigma_v - d\sigma_v)B_z + 2\left(\frac{dz}{\cos\alpha}\right) \cdot \tau_s \cos\alpha + 2\left(\frac{dz}{\cos\alpha}\right)\sigma_{ns}\sin\alpha, \quad (1)$$

where $B_z = b + 2z\tan\alpha$, γ is the gravity of the fill material, and σ_v is the vertical stress.

As shown in Figure 3, the shear stress can be expressed as follows:

$$\tau = (\sigma_h - \sigma_3)\tan\theta. \quad (2)$$

According to the geometric position relation in the stress Mohr circle, the following formulations can be obtained:

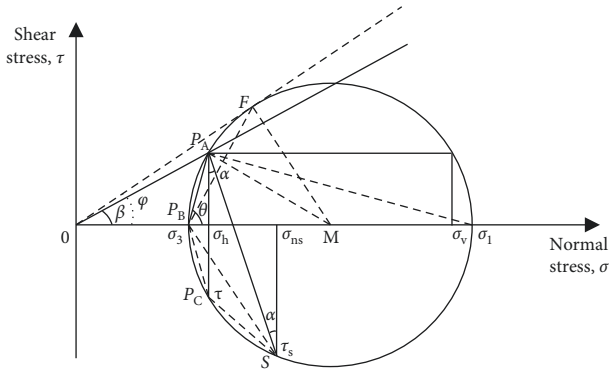

Figure 3: Mobilization of shear stress in the Mohr circle.

$$\begin{cases} \sigma_h = \sigma_1 \cos^2\theta + \sigma_3 \sin^2\theta, \\ \sigma_v = \sigma_1 \sin^2\theta + \sigma_3 \cos^2\theta, \end{cases} \quad (3)$$

where σ_h and σ_v are the horizontal/vertical stresses of the soil arch, respectively; σ_1 and σ_3 are the major and minor principle stresses, respectively; and θ is the angle of σ_1 related to the horizontal direction.

The lateral active Earth pressure coefficient is defined as follows:

$$K_a = \frac{\sigma_3}{\sigma_1} = \tan^2\left(45 - \frac{\varphi}{2}\right). \quad (4)$$

When equation (3) is divided by σ_1, it becomes

$$\begin{cases} \frac{\sigma_h}{\sigma_1} = \cos^2\theta + K_a \sin^2\theta, \\ \frac{\sigma_v}{\sigma_1} = \sin^2\theta + K_a \cos^2\theta. \end{cases} \quad (5)$$

If the lateral Earth pressure coefficient is defined as the ratio of lateral stress to vertical stress, one can get the following:

$$K = \frac{\sigma_h}{\sigma_v} = \frac{\cos^2\theta + K_a \sin^2\theta}{\sin^2\theta + K_a \cos^2\theta} = \frac{1 + K_a \tan^2\theta}{\tan^2\theta + K_a}. \quad (6)$$

Here, the shear stress can be formulated as follows:

$$\tau = \sigma_h \tan\beta. \quad (7)$$

While $\sigma = \sigma_1 \cos^2\theta + \sigma_3 \sin^2\theta$ is divided by σ_3 and then substituted into equation (7), the following relationship can be established:

$$\tan\beta = \frac{(1 - K_a)\tan\theta}{1 + K_a \tan^2\theta}. \quad (8)$$

So, the shear stress of equation (7) can be reformulated as follows:

$$\tau = K\sigma_v \tan\beta = \frac{K\sigma_v(1 - K_a)\tan\theta}{1 + K_a \tan^2\theta}. \quad (9)$$

Assume that

$$C_1 = \frac{K(1 - K_a)\tan\theta}{1 + K_a \tan^2\theta}. \quad (10)$$

The angle θ is determined by the geometric relation illustrated in Figure 2; when R is defined as the deflection radius, it can be expressed as follows:

$$R = \frac{B_z}{2\cos\theta} = \eta + \frac{B_z \tan\theta}{2}. \quad (11)$$

Here,

$$\eta = \frac{B_z \tan(45^\circ - (\theta/2))}{2}. \quad (12)$$

Likewise, the normal stress acting on the idealized inclined slip surface a′b at a depth z to the top surface can be expressed as follows:

$$\sigma_{ns} = \sigma_1 \cos^2(\theta - \alpha) + \sigma_3 \sin^2(\theta - \alpha), \quad (13)$$

where α is the angle between the inclined slip surface and the vertical direction.

When equation (13) is divided by σ_1 and the resulting equation is substituted in equation (5), the following relation can be established:

$$\sigma_{ns} = \frac{\cos^2(\theta - \alpha) + K_a \sin^2(\theta - \alpha)}{\sin^2\theta + K_a \cos^2\theta}\sigma_v. \quad (14)$$

Let

$$C_2 = \frac{\cos^2(\theta - \alpha) + K_a \sin^2(\theta - \alpha)}{\sin^2\theta + K_a \cos^2\theta}. \quad (15)$$

Then, the shear stress $\tau_s = (\sigma_{ns} - \sigma_h)\cot\alpha - \tau$ can be reorganized to be as follows:

$$\tau_s = [(C_2 - K)\cot\alpha - C_1]\sigma_v. \quad (16)$$

Let

$$C_3 = (C_2 - K)\cot\alpha - C_1. \quad (17)$$

Substituting equations (14) and (15) into equation (1) and dividing both sides by d_z, one can get the following:

$$\frac{d\sigma_v}{dz} - \frac{2C_3 + 2C_2 \tan\alpha}{b + 2z\tan\alpha}\sigma_v = -\gamma. \quad (18)$$

The solution of the vertical stress can be expressed as follows:

$$\sigma_v = \left[C_4 - \frac{\gamma(b + 2z\tan\alpha)^{(1 - C_5)}}{2(1 - C_5)\tan\alpha}\right](b + 2z\tan\alpha)^{C_5}. \quad (19)$$

Let

$$C_5 = \frac{(2C_3 + 2C_2 \tan\alpha)}{2\tan\alpha}. \quad (20)$$

where C_4 is an unknown parameter. As illustrated in Figure 1, when $z = H$ and $\sigma_v = q$, then one can get the following:

$$C_4 = q(b + 2H\tan\alpha)^{-C_5} + \frac{\gamma(b + 2H\tan\alpha)^{(1 - C_5)}}{2(1 - C_5)\tan\alpha}. \quad (21)$$

3. Equivalent Geomembrane Effect

The tension of the geosynthetic is dependent on the deflection, and the maximum tensile strain is recognized to occur at the edges of the subsiding basin [21, 22]. It is acceptable that the geomembrane effect would be more predominant due to the increasing differential settlement. In Figure 4, the reinforcement layer consists of three segments, the anchorage section on the supporting soil, the transition section due to tensile elongation, and the deflection section within the subsided area. To simplify the analysis, the shape of the deflected geosynthetic layer is idealized to be a fixed form, accompanied with the assumption that the vertical stresses on soil and reinforcement are uniformly distributed (see Figure 5). Theoretically, the load acting on the geosynthetic layer (within the deflected span) equals to the arch zone weight deducting the friction from the adjacent stationary fill mass and also equals to the conjunction of the geomembrane lift capacity and resistance from the compressible subsoil.

Refining from the analytical models proposed by Villard and Briançon [22] and Feng et al. [29], a similar evaluation method for the geomembrane effect of reinforcement is also presented in this study. In Figure 4, the geosynthetic layer deflects due to a uniform load q_g acting on its upper surface, but generates a maximum tension T_c at the edge of the subsided area. The tangent angle at point C (in Figure 4) of the reinforcement is φ_c. At a random point M within the deflection, its tensile force is T_M, with an oblique angle of φ_M. Adopting the Coulomb friction law (Figure 6) to define the interface friction between the soil and geosynthetic, one obtains the following expression:

$$\tau = \begin{cases} \dfrac{u}{u_0}(\sigma_n \tan\varphi_0), & (u < u_0), \\ \sigma_n \tan\varphi_0, & (u \geq u_0), \end{cases} \quad (22)$$

where u and u_0 are the relative displacement and critical relative displacement between the soil and geosynthetic,

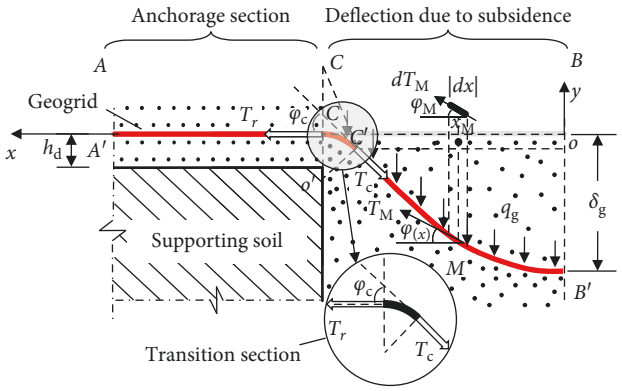

Figure 4: Deflection of the horizontal geosynthetic reinforcement due to localized subsiding.

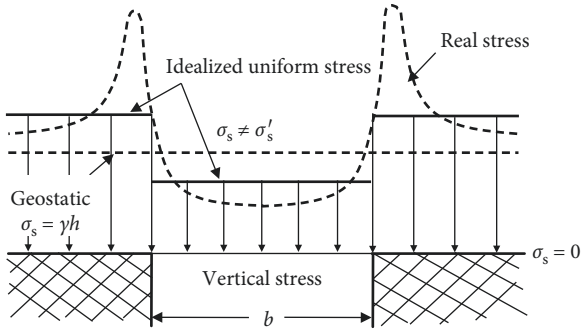

Figure 5: Distribution of overlying vertical stress at the bottom of embankment.

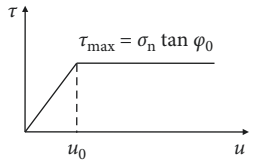

Figure 6: Coulomb friction law.

respectively; φ_0 is the friction angle between the soil and geosynthetic; and σ_n is the normal stress.

Checking a microelement of dl (see Figure 7), the equilibrium relationships can be established as

$$\begin{cases} T_{h(x)} = T_{M(x)} \cdot \cos \varphi_{(x)}, \\ T_{v(x)} = T_{M(x)} \cdot \sin \varphi_{(x)}, \\ y'(x) = \tan \varphi_{(x)} = \dfrac{dy}{dx}, \\ T_{v(x)} = T_{h(x)} y'(x), \end{cases} \tag{23}$$

where $T_{M(x)}$, $T_{v(x)}$, and $T_{h(x)}$ are the tensile, vertical, and horizontal tensile component forces, respectively, of the geosynthetic at point M; $\varphi_{(x)}$ is the inclination angle to the

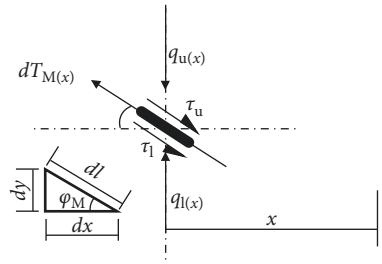

Figure 7: Mechanical analysis of a deflected element of the geosynthetic.

horizontal direction; and $y(x)$ and $y'(x)$ are the deformed deflection of the geosynthetic and its derivative form at point M with an abscissa position x to the midpoint.

In order to make a further simplification, an assumed relationship can be established as follows:

$$\begin{cases} \tau_u = \tau, \\ \tau_l = k_1 \tau_u, \quad (0 \le k_1 \le 1), \end{cases} \tag{24}$$

where τ_u and τ_l are the upper and lower friction strength of the interfaces between the soil and geosynthetic, respectively; k_1 is the reduction coefficient of the lower interface to the upper one.

Assuming that $q_{g(x)} = q_{u(x)} - q_{l(x)}$, where $q_{g(x)}$ is the equivalent geomembrane stress upward due to deflection, $q_{u(x)}$ and $q_{l(x)}$ are the upper and lower vertical stresses, respectively, acting on the geosynthetic element. The following relationship can be established:

$$\begin{cases} dT_{h(x)} - (1 + k_1)\tau\, dl \cdot \cos \varphi_M = 0, \\ dT_{v(x)} - q_{g(x)} dx - (1 + k_1)\tau\, dl \cdot \sin \varphi_M = 0. \end{cases} \tag{25}$$

Then, one can obtain

$$\tau = \frac{dT_{h(x)}}{(1 + k_1) dx}, \tag{26}$$

and

$$\frac{dT_{v(x)}}{dx} - q_{g(x)} - (1 + k_1)\tau \cdot \tan \varphi_M = 0. \tag{27}$$

Deriving the third term in equation (23), it can be reformulated as

$$\frac{dT_{v(x)}}{dx} = \frac{dT_{h(x)}}{dx} y'(x) + T_h y''(x). \tag{28}$$

Substituting equations (26) and (28) in equation (27) yields

$$q_{g(x)} = T_{h(x)} y''(x). \tag{29}$$

Originally, there is also a relationship

$$T_{h(x)} = J_g \varepsilon_{(x)} \cos \varphi_{(x)} = J_g \frac{\varepsilon_{(x)}}{\sqrt{1 + y'^2(x)}}, \tag{30}$$

where $\varepsilon_{(x)}$ is the tensile strain of the selected analysis element and J_g is the tensile stiffness of the geosynthetic. Then, the geomembrane effect of equation (29) can be reformulated as

$$q_{g(x)} = T_{h(x)} y''(x) = J_g \frac{\varepsilon_{(x)} y''(x)}{\sqrt{1 + y'^2(x)}}. \quad (31)$$

Also, the tensile strain at point M can be expressed as

$$\varepsilon_{(x)} = \frac{\sqrt{1 + y'^2(x)}}{u'(x)}, \quad (32)$$

where $u'(x)$ is the derivative form of the geosynthetic displacement at point M. Substituting equation (32) in equation (31) yields

$$q_{g(x)} = T_h y''(x) = J_g \frac{u'(x) y''(x)}{1 + y'(x)^2}. \quad (33)$$

The overlying load of the geosynthetic layer under soil arching is averaged in the range of the subsided area and yields

$$q_u = \frac{2J_g}{b} \int_0^{b/2} \left(\frac{u'(x) y''(x)}{1 + y'(x)^2} + k_s y(x) \right) dx, \quad (34)$$

where k_s is the reaction coefficient of foundation soil.

In theory, equation (19) is equal to equation (34). In this study, the parabolic shape of the geosynthetic is adopted to evaluate the geomembrane effect due to localized sinking. The only uncertainty is how to determine the deflection of the geosynthetic with a particular tensile stiffness.

As the transition zone between the deflection section and the anchorage section, there is an angle change of tensile forces, which is accompanied by the elongation of the installed geosynthetic. Combining the above effects yields

$$T_{r_0} = T_c e^{-\varphi_c \tan \varphi}, \quad (35)$$

where T_c and T_{r_0} are the tensile force at point C of the deflected section and the tensile force of anchorage section, respectively; φ_c is the inclination angle of the tangent direction of the deflected geosynthetic; and φ is considered to be a comprehensive friction angle of the geosynthetic and soil. Villard and Briançon [22] suggested that this angle equals to the lower friction angle of the geosynthetic and soil. Occasionally, there exists a relationship that $\varphi_c + \theta = \pi/2$, which connects the deflection section and the anchorage section.

As illustrated in Figure 8, the anchoring behavior of the geosynthetic should be considered in two cases. One is that the relative displacement between the geosynthetic and soil does not exceed the critical displacement as defined in Figure 6, and the other is that the relative displacement between the geosynthetic and soil within the anchorage section has reached the critical state.

Selecting an element dr at a distance r to the edge point C of the subsided area, the force balance relation in the horizontal direction can be formulated as follows:

$$dT_r = -\left(\tau_{up} + \tau_{low}\right) dr, \quad (36)$$

where τ_{up} and τ_{low} are the upper and lower friction stresses, respectively, of the interfaces between the geosynthetic and soil within the anchorage section. To simplify the derivation, cohesion of interface is not considered, and the Coulomb friction law is adopted. Under a specific relative displacement U between the geosynthetic and soil, the friction can be formulated as follows:

$$\tau_{up/low} = \begin{cases} \sigma_0 \tan \phi_{up/low} \dfrac{U}{u_0}, & (U < u_0), \\ \sigma_0 \tan \phi_{up/low}, & (U \geq u_0), \end{cases} \quad (37)$$

where σ_0 is the normal stress acting on the anchorage length of the geosynthetic; ϕ_{up} and ϕ_{low} are the upper and lower friction angles, respectively, of interfaces within the anchorage section.

Then, equation (36) can be reformulated as

$$dT_r = \begin{cases} -\sigma_0 \left(\tan \phi_{up} + \tan \phi_{low}\right) \dfrac{U}{u_0} dr, \\ -\sigma_0 \left(\tan \phi_{up} + \tan \phi_{low}\right) dr. \end{cases} \quad (38)$$

Considering the relation $T_r = J_g \varepsilon = -J_g dU/dr$, when the relative displacement between the geosynthetic and soil does not exceed the critical condition, as illustrated in Figure 8(a), equations (36) to (38) can be deduced to be

$$\frac{d^2U}{dr^2} = \beta^2 U, \quad (39)$$

where $\beta = \sigma_0 (\tan \phi_{up} + \tan \phi_{low}) / (J_g u_0)$. The general solution of equation (39) is

$$U = \frac{C_1}{2} \left(e^{\beta r} - e^{-\beta r}\right) + \frac{C_2}{2} \left(e^{\beta r} + e^{-\beta r}\right), \quad (40)$$

where C_1 and C_2 are the constant coefficients depending on boundary conditions. When $r = L$ (the anchorage length) and $U = 0$; when $r = 0$ and $T_r = T_{r_0}$, and one can get

$$U = \frac{T_{r_0} \left(e^{\beta(L-r)} - e^{-\beta(L-r)}\right)}{J_g \beta \left(e^{\beta L} + e^{-\beta L}\right)}. \quad (41)$$

Now, the displacement of point C can be solved to be

$$U_C = \frac{T_{r_0} \left(e^{\beta L} - e^{-\beta L}\right)}{J_g \beta \left(e^{\beta L} + e^{-\beta L}\right)} \Longrightarrow \left. \frac{T_{r_0}}{J_g \beta} \right|_{L/u_0 \, (\longrightarrow \infty)}. \quad (42)$$

When the relative displacement between the geosynthetic and soil within the anchorage section partially reaches the critical state, the anchorage section AC should be divided into two parts, the AD segment and the DC segment. The AD segment shares the same deducing procedure as derived above. For the DC segment, one can get

$$T = T_{r_0} - q_0 r = J_g \varepsilon = -J_g \frac{dU}{dr}, \quad (43)$$

where ε is the tensile strain of the geosynthetic at distance r to point C; and $q_0 = \sigma_0 (\tan \phi_{up} + \tan \phi_{low})$.

Then, the solution can be deduced to be

$$U = \frac{T_{r_0} r}{J_g} + \frac{q_0 r^2}{2J_g} + U_C. \quad (44)$$

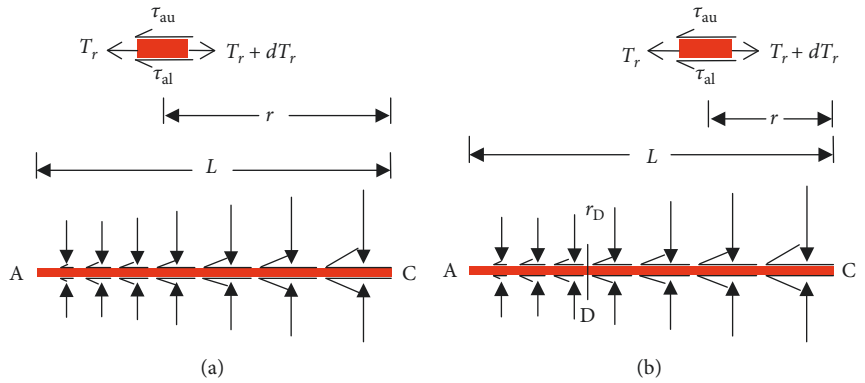

Figure 8: Analysis of the geosynthetic anchorage section: (a) does not reach critical relative displacement; (b) partially in critical displacement condition.

For the dividing point D, when $r = r_D$, there exists relations, $T_N = T_0$ and $U_D = u_0$. Therefore, the dividing point position can be determined by

$$r_D = \frac{T_{r_0} - T_0}{q_0}, \tag{45}$$

where $T_0 = u_0 J_g \beta$.

Then, the relationship between the displacement and tensile forces can be established as

$$U_C = u_0 - \frac{\left(T_0^2 - T_{r_0}^2\right)}{2J_g q_0}. \tag{46}$$

According to a fixed analytical model, such as definite mechanical properties of reinforcement materials and soils, as well as given geometries, the only unknown is the deflection of the geosynthetic. Obviously, the iterative method should be utilized to solve the above question, and some simplified conditions need to be assumed. For example, the stress diffusion in the horizontal direction is not considered, and load transfer adjustment only occurs in the vertical direction. Moreover, the separation between the geosynthetic and soil is not allowed, and the stress and displacement along the geosynthetic layer are continuously coordinated. Integrating the entire derivation process, the iterative calculation procedure can be illustrated as in Figure 9. To begin with an arbitrary original setting of the $u'_{(x)}$ (e.g., a linear expression), the calculation starts with a fixed geosynthetic trajectory. Once the deflection of the geosynthetic is determined, the tensile strain can be deduced, as well as the equivalent applying stress. Meanwhile, the overlying load that is averaged within the subsided area can be calculated, and a comparison is made to the previous geomembrane effect. If the deviation is within the acceptable range (such as one thousandth), the iterative solution ends. Then, the anchorage section can be evaluated in two cases.

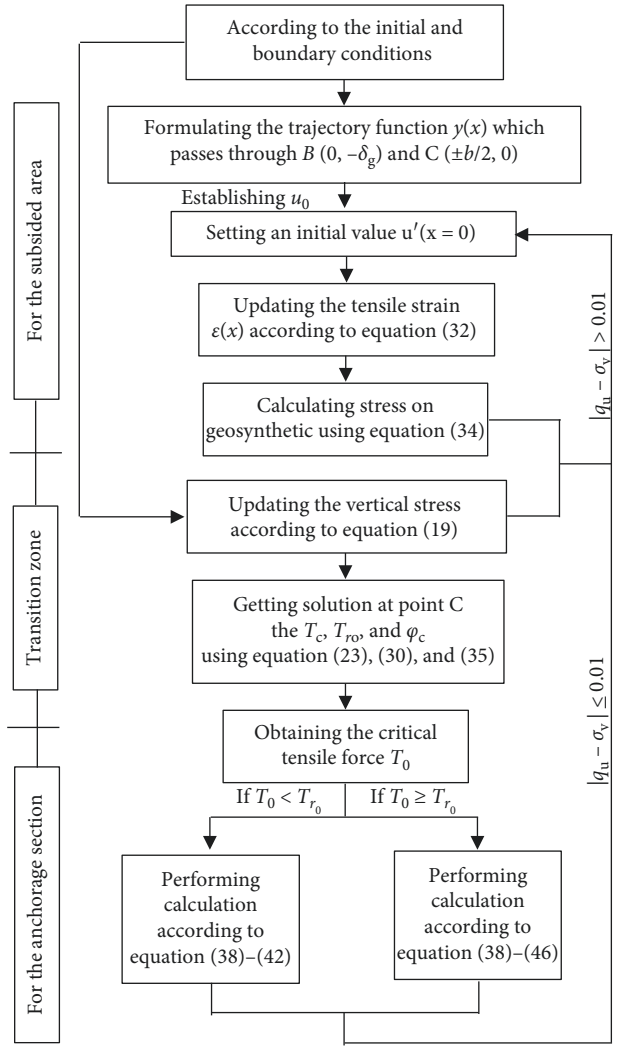

Figure 9: Iterative calculation procedure of the proposed method.

4. Model Validation and Discussion

This part compares the results of the present method and a full-scale experiment test, as well as the results of the analytical methods proposed by Villard and Briançon [22] and Feng et al. [29]. The test was carried out by a sudden deflation of an air balloon to investigate the reinforcing behavior of the basal geosynthetic (see Figure 10). Detailed information about the physical model is as follows: the cohesionless fill height is 0.5 m with gravity 17 kN/m^3, the

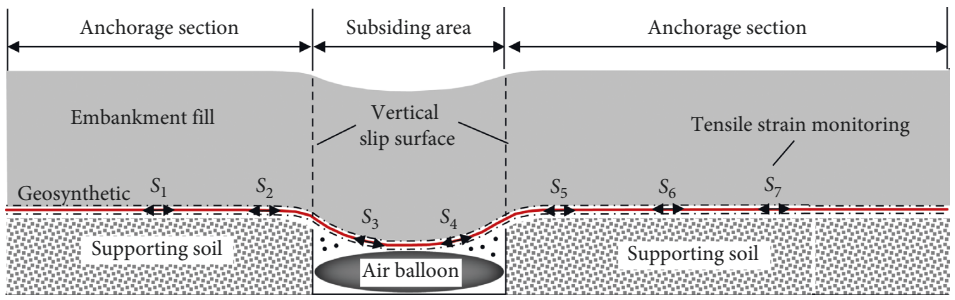

Figure 10: The air balloon trapdoor test carried out by Villard and Briançon [22].

width and height of the balloon are 2.0 m and 0.25 m, respectively. A single layer of the geosynthetic is installed on the balloon, with more than 2.0 m of the anchorage length. The ultimate tensile force is 125 kN/m with regard to the tensile strain of 12%. The model achieves the effect of basement hollowing by means of airbag deflation. Therefore, there is no support from the underneath foundation soil, indicating that the geosynthetic layer fully accommodates the upper embankment load. The relevant calculation parameters are shown in Table 1, and the tensile strains are compared, as illustrated in Figure 11.

In Figure 11, the strains of the deflected geosynthetic calculated by the present method, the Villard and Briançon [22] method, and the Feng et al.'s [29] method are all close to the test results. Due to the lack of settlement data on the embankment surface, the calculations are all founded on the vertical slip surface assumption. Obviously, the present method yields the maximum tensile strains within the subsided area, and they are closer to the results observed five months after the end of the experiment. The Villard and Briançon [22] method does not consider the interface friction of geosynthetic and soil within the subsided area, so the peak tensile strain is the smallest and the length of anchorage is the smallest, too. Feng et al. [29] argued that ignoring the upper friction results in undervaluation of maximum geosynthetic strain, and their method obtains a relatively higher geomembrane effect. However, the overlying vertical load and its distribution significantly influence the geomembrane effect of the geosynthetic. Feng et al. [29] adopted the Terzaghi's [8] fully mobilized arching theory to calculate the vertical stress on the geosynthetic layer, so the load obtained is less than that of the present method, as well as the corresponding geosynthetic tensile strains.

The above validation is based on the vertical slip surface condition. However, for the localized sinking of the base, the subsidence on top is enlarged and the width is greater than the base. In this case, the overlying load of the basal reinforcement is different from that of the vertical slip surface as previously assumed. Under a fixed subsidence at the fill base, when the inclined angle of slip surface decreases from almost 90° to 45° – (φ/2) (φ is the internal friction angle of the fill), the overlying stress acted on the basal geosynthetic is variable as is shown in Figure 12.

This section compares the results of the analytical calculations by this study and a rubber water bag trapdoor test conducted by Miao et al. [35]. Different from the Villard and Briançon's [22] test, Miao et al. [35] adopted a graded-drainage subsidence manner to evaluate the reinforcing mechanism of the geosynthetic. The advantage is that the changes of displacement and stress of embankment and the response of reinforcing behavior can be recorded stepwise. Although the cohesion of the embankment fill may have influence for the ease of comparison, it is also worth trying to analyze the change of overlying load. Detailed information about the experimental model is as follows: the fill height is 0.6 m with the gravity of 18.8 kN/m^3 and the width and height of the rubber water bag are 1.0 m and 0.30 m,

Table 1: Parameters in the calculation process.

Parameters	Villard et al.'s balloon trapdoor test	Miao et al.'s water bag trapdoor test		
δ_g (cm)	22.0	0.3	3.2	8.0
U_0 (cm)	5.0		5.0	
K_1	0.00	0.96	0.60	0.0
K_s (MPa)	30		15	
φ_0 (°)	25		20	
ϕ_{up} (°)	30		25	
ϕ_{low} (°)	25		20	
σ_0 (kPa)	8.50		11.28	

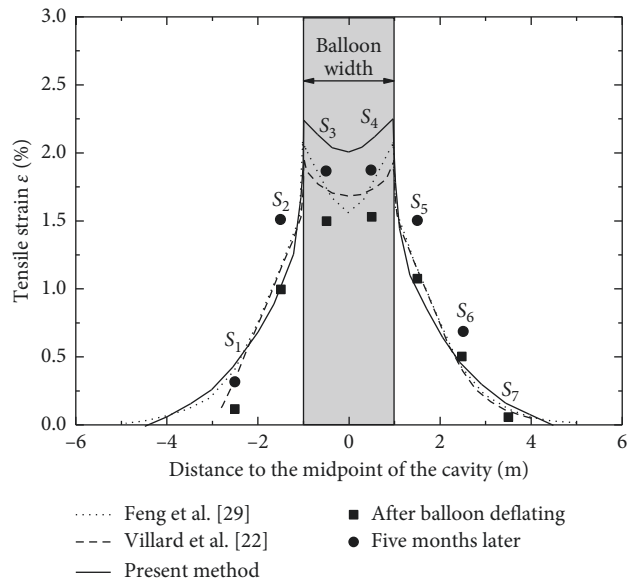

Figure 11: Comparison of test tensile strains and calculated results.

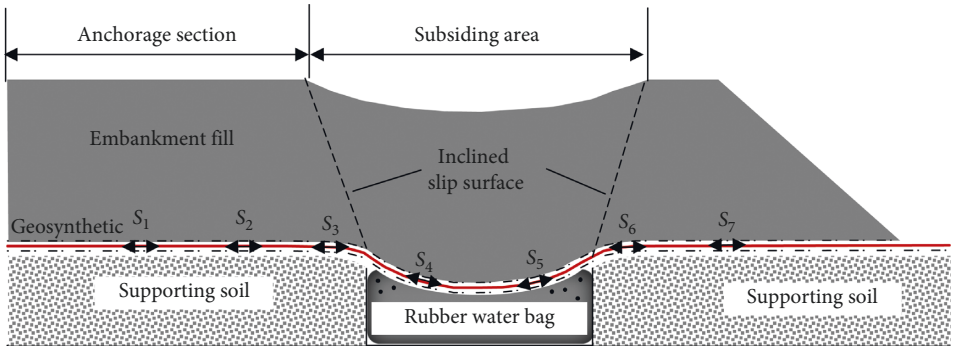

Figure 12: The rubber water bag trapdoor test conducted by Miao et al. [35].

respectively. A single layer of the geosynthetic is installed at 5.0 cm on the rubber water bag, with more than 1.0 m of anchorage length. The ultimate tensile force is 42.3 kN/m with regard to the tensile strain of 10.9 %. The subsidence of the rubber bag is controlled by the water discharge.

Due to the relatively low embankment height, frictional arching models proposed by Terzaghi [8] and Handy [36] are selected to make a comparison. As shown in Figure 13, ranking the stresses with the increasing local subsidence, it is clear that the Terzaghi method obtains moderate stresses while the Handy method yields slightly larger ones, but all remain unchanged. With increasing subsiding width from the observation of embankment surface settlement, i.e., increasing inclined angles of the slip surfaces, the load acting on the geosynthetic decreases. Although there are some deviations from the measured data, the trend of the change coincides very well. It is very difficult to obtain the true reduction coefficient, so the reduction coefficient (Table 1) here is replaced by the ratio of geosynthetic deflection to the maximum settlement of the rubber water bag.

Based on three different local subsidence (see Figure 14), the tensile strains of the geosynthetic vary with different overlying loads, accompanied with the different subsidence on the fill surface. Through comparison, it can be seen that this method can predict the magnitude and distribution of tensile strains of the geosynthetic well according to different deflections. The analytical model is based on a symmetric condition, while the validation test is asymmetric, so the difference exists but is acceptable.

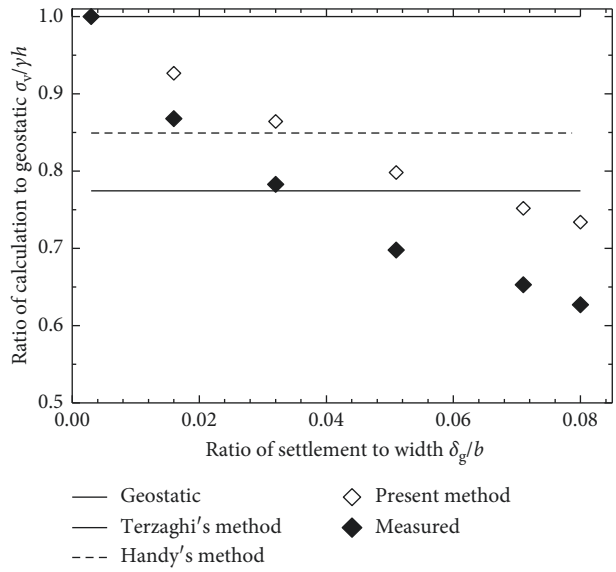

Figure 13: Comparison of load on the geosynthetic layer due to local subsidence.

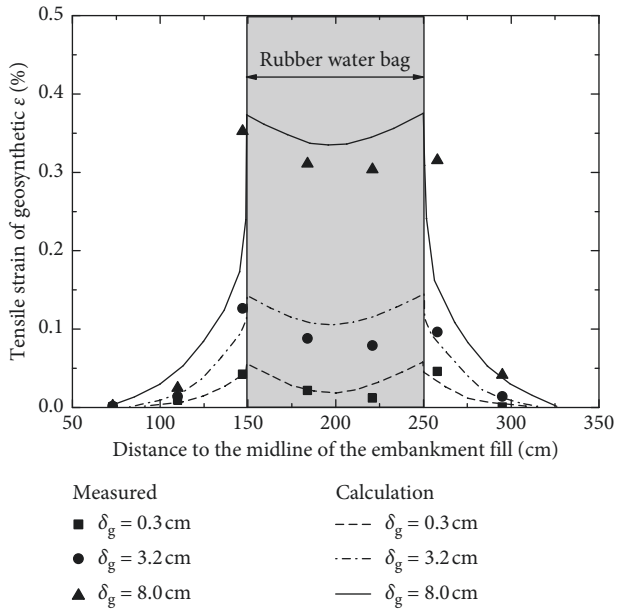

Figure 14: Comparison of tensile strains and calculated results of the Miao et al.'s test.

5. Conclusions

In this study, a semiempirical analyzing method, applying the developing arching effect based on mobilized shear stress along inclined slip surface, is presented to evaluate the geomembrane effect of the basal geosynthetic due to localized subsidence. Through comparison and discussion, the following conclusions are obtained:

(1) Based on traditional definition of lateral Earth pressure coefficient, an improved definition method considering deflection of subsided soil within the subsided area is proposed. In derivation, the influence of mobilized shear stress along slip surface on arching and interface friction between a geosynthetic

and fill can be quantitatively evaluated, which can be solved by an iterative method.

(2) The present method is validated reasonable by two physical model tests, as well as results calculated by some current methods. For the overlying load on the geosynthetic, the present method obtains variable stresses according to variable deflections with a good coincidence. Considering the interface friction between the geosynthetic and soil and the incomplete arching effect, the present method obtains maximum tensile strains against the other two methods.

(3) Influence of the loading pattern along the geosynthetic layer and cohesion of the fill material on the reinforcing mechanism of the geosynthetic are not discussed in this study. Further studies, including numerical simulations, simplifications, and more experimental tests, are strongly recommended to gain better understanding of the validity and application of the present method.

Data Availability

The experimental data used to support the findings of this study are included within the article. And other previously reported data supporting this article are from the outcomes of publicly published papers. Those prior studies (and datasets) have been cited at relevant places within the text as references. The authors agree to share the data of this paper and allow other researchers to verify the results of this article, replicate the analysis, and conduct secondary analyses.

Conflicts of Interest

The authors declare that they have no conflicts of interest.

Acknowledgments

The authors acknowledge and appreciate the financial support provided by the National Natural Science Foundation of China (Project nos. 51508279; 51478054; 51508278) and the Jiangsu Provincial Natural Science Fund Projects (BK20150885). Moreover, the work was also supported by the Open Fund of Key Laboratory of Road Structure and Material of Ministry of Transport (Changsha University of Science & Technology, kfj180303), the Systematic Project of Guangxi Key Laboratory of Disaster Prevention and Structural Safety (2016ZDK005), and the Ministry of Housing and Urban-Rural Development of the People's Republic of China (2018-K4-008).

References

[1] J. Zhang, J. Peng, J. Zheng, and Y. Yao, "Characterisation of stress and moisture-dependent resilient behaviour for compacted clays in South China," *Road Materials and Pavement Design*, pp. 1–14, 2018.

[2] X. Zhang, J. Yang, Y. Zhang, and Y. Gao, "Cause investigation of damages in existing building adjacent to foundation pit in construction," *Engineering Failure Analysis*, vol. 83, pp. 117–124, 2018.

[3] Y. Zhao, C. Liu, Y. Zhang, J. Yang, and T. Feng, "Damaging behavior investigation of an operational tunnel structure induced by cavities around surrounding rocks," *Engineering Failure Analysis*, vol. 99, pp. 203–209, 2019.

[4] J. Li, J. H. Zhang, G. P. Qian, J. L. Zheng, and Y. Q. Zhang, "Three-dimensional simulation of aggregate and asphalt mixture using parameterized shape and size gradation," *Journal of Materials in Civil Engineering*, vol. 31, no. 3, article 04019004, 2019.

[5] W. Lu, L. Miao, J. Zhang, Y. Zhang, and J. Li, "Characteristics of deformation and damping of cement treated and expanded polystyrene mixed lightweight subgrade fill under cyclic load," *Applied Sciences*, vol. 9, no. 1, p. 167, 2019.

[6] Y. X. Zhang, Y. Fang, W. H Lu et al., "Shrinkage behavior influence of strain hardening cementitious composites," *Structural Concrete*, 2019, In press.

[7] Y. X. Zhang, C. Liu, W. H. Lu, H. B. Xie, and H. Peng, "Comparative study of RC members with strengthening using strain hardening cementitious composite and fiber reinforced mortar," *Journal of Testing and Evaluation*, vol. 47, no. 1, pp. 35–42, 2019.

[8] K. Terzaghi, *Theoretical Soil Mechanics*, Wiley, New York, NY, USA, 1943.

[9] B. K. Low, S. K. Tang, and V. Choa, "Arching in piled embankments," *Journal of Geotechnical Engineering*, vol. 120, no. 11, pp. 1917–1938, 1994.

[10] S. J. M. Van Eekelen, A. Bezuijen, and A. F. Van Tol, "An analytical model for arching in piled embankments," *Geotextiles and Geomembranes*, vol. 39, pp. 78–102, 2013.

[11] S. W. Abusharar, J.-J. Zheng, B.-G. Chen, and J.-H. Yin, "A simplified method for analysis of a piled embankment reinforced with geosynthetics," *Geotextiles and Geomembranes*, vol. 27, no. 1, pp. 39–52, 2009.

[12] W. Lu and L. Miao, "A simplified 2-D evaluation method of the arching effect for geosynthetic-reinforced and pile-supported embankments," *Computers and Geotechnics*, vol. 65, pp. 97–103, 2015.

[13] F. Gu, X. Luo, R. Luo, R. L. Lytton, E. Y. Hajj, and R. V. Siddharthan, "Numerical modeling of geogrid-reinforced flexible pavement and corresponding validation using large-scale tank test," *Construction and Building Materials*, vol. 122, pp. 214–230, 2016.

[14] S.-J. Feng, S.-G. Ai, and H. X. Chen, "Estimation of arching effect in geosynthetic-reinforced structures," *Computers and Geotechnics*, vol. 87, pp. 188–197, 2017.

[15] M. Wang, Y. X. Feng, and M. Jao, "Stability of geosynthetic-reinforced soil above a cavity," *Geotextiles and Geomembranes*, vol. 14, no. 2, pp. 95–109, 1996.

[16] S. K. Shukla, J. G. Loughran, and N. Sivakugan, "Stress within a cohesionless granular fill in a storage vessel with sloping walls during initial static loading," *Powder Technology*, vol. 192, no. 3, pp. 389–393, 2009.

[17] T. Eskişar, J. Otani, and J. Hironaka, "Visualization of soil arching on reinforced embankment with rigid pile foundation using X-ray CT," *Geotextiles and Geomembranes*, vol. 32, no. 32, pp. 44–54, 2012.

[18] J. H. Zhang, J. H. Peng, J. L. Zheng, L. L. Dai, and Y. S. Yao, "Prediction of resilient modulus of compacted cohesive soils in South China," *International Journal of Geomechanics*, vol. 19, no. 7, 2019.

[19] J. P. Giroud, R. Bonaparte, J. F. Beech, and B. A. Gross, "Design of soil layer-geosynthetic systems overlying voids,"

Geotextiles and Geomembranes, vol. 9, no. 1, pp. 11–50, 1990.

[20] BSI (British Standards Institution), *Code of Practice for Strengthened/Reinforced Soil and Other Fills. BS8006*, BSI (British Standards Institution), London, UK, 2016.

[21] J. Han and M. A. Gabr, "Numerical analysis of geosynthetic-reinforced and pile-supported earth platforms over soft soil," *Journal of Geotechnical and Geoenvironmental Engineering*, vol. 128, no. 1, pp. 44–53, 2002.

[22] P. Villard and L. Briançon, "Design of geosynthetic reinforcements for platforms subjected to localized sinkholes," *Canadian Geotechnical Journal*, vol. 45, no. 2, pp. 196–209, 2008.

[23] A. Huckert, L. Briançon, P. Villard, and P. Garcin, "Load transfer mechanisms in geotextile-reinforced embankments overlying voids: experimental and analytical approaches," *Geotextiles and Geomembranes*, vol. 44, no. 3, pp. 442–456, 2016.

[24] Y. Yu and R. J. Bathurst, "Influence of selection of soil and interface properties on numerical results of two soil-geosynthetic interaction problems," *International Journal of Geomechanics*, vol. 17, no. 6, article 04016136, 2017.

[25] R. D. Espinoza, "Soil-geotextile interaction: evaluation of membrane support," *Geotextiles and Geomembranes*, vol. 13, no. 5, pp. 281–293, 1994.

[26] J. P. Gourc and P. Villard, "Reinforcement by membrane effect: application to embankments on soil liable to subsidence," in *Proceedings of the 2nd Asian Geosynthetics Conference, ASIA 2000*, vol. 1, pp. 55–72, Kuala Lumpur, Malaysia, May 2000.

[27] P. Villard, A. Huckert, and L. Briançon, "Load transfer mechanisms in geotextile-reinforced embankments overlying voids: numerical approach and design," *Geotextiles and Geomembranes*, vol. 44, no. 3, pp. 381–395, 2016.

[28] F. Gu, Y. Zhang, X. Luo, R. Luo, and R. L. Lytton, "Impact of geogrid on cross-anisotropy and permanent deformation of unbound granular materials," *Transportation Research Record: Journal of the Transportation Research Board*, vol. 2580, no. 1, pp. 34–46, 2016.

[29] S.-J. Feng, S.-G. Ai, and H.-X. Chen, "Membrane effect of geosynthetic reinforcement subjected to localized sinkholes," *Canadian Geotechnical Journal*, vol. 55, no. 9, pp. 1334–1348, 2018.

[30] P. J. Naughton, "The significance of critical height in the design of piled embankments," in *Proceedings of the Geo-Denver 2007, New peaks in Geotechnics, ASCE GSP 172, Soil Improvement*, pp. 18–21, Denver, CO, USA, February 2007.

[31] H. G. Kempfert, C. Gobel, D. Alexiew, and C. Heitz, "German recommendations for the reinforced embankments on pile-similar elements," in *Proceedings of the Third European Conference on Geosynthetics*, pp. 279–284, Munich, Germany, 2004.

[32] R. P. Chen, Y. M. Chen, J. Han, and Z. Z. Xu, "A theoretical solution for pile-supported embankments on soft soils under one-dimensional compression," *Canadian Geotechnical Journal*, vol. 45, no. 5, pp. 611–623, 2008.

[33] J. G. Collin, "Column supported embankment design considerations," in *Proceedings of the 52nd Annual Geotechnical Engineering Conference*, pp. 51–78, University of Minnesota, Minneapolis, MI, USA, February 2004.

[34] D. P. Krynine, "Discussion of "stability and stiffness of cellular cofferdams" by Karl Terzaghi," *Transactions*, vol. 110, pp. 1175–1178, 1945.

[35] L. Miao, F. Wang, J. Han, and W. Lv, "Benefits of geosynthetic reinforcement in widening of embankments subjected to foundation differential settlement," *Geosynthetics International*, vol. 21, no. 5, pp. 321–332, 2014.

[36] R. L. Handy, "The arch in soil arching," *Journal of Geotechnical Engineering*, vol. 111, no. 3, pp. 302–318, 1985.